Extension of the mapped Fourier method to time-dependent problems

Ulrich Kleinekathöfer* and David J. Tannor
Department of Chemical Physics, Weizmann Institute of Science, 76100 Rehovot, Israel
(Received 12 April 1999)

A numerical method is described for integration of the time-dependent Schrödinger equation within the presence of a Coulomb field. Because of the singularity at $r=0$, the wave packet has to be represented on a grid with a high density of points near the origin; at the same time, because of the long-range character of the Coulomb potential, the grid must extend to large values of r. The sampling points are chosen, following E. Fattal, R. Baer, and R. Kosloff [Phys. Rev. E **53**, 1217 (1996)], using a classical phase space criterion. Following those workers, the unequally spaced grid points are mapped to an equally spaced grid, allowing use of fast Fourier transform propagation methods that scale as $N \ln N$, where N is the number of grid points. As a first test, eigenenergies for the hydrogen atom are extracted from short-time segments of the electronic wave-packet autocorrelation function; high accuracy is obtained by using the filter-diagonalization method. As a second test, the ionization rate of the hydrogen atom resulting from a half-cycle pulse is calculated. These results are in excellent agreement with earlier calculations. [S1063-651X(99)14210-7]

PACS number(s): 02.70.Jn, 31.15.−p, 32.80.Rm

I. INTRODUCTION

Numerous different approaches have been developed to solve the time-dependent Schrödinger equation. Fast Fourier transform (FFT) methods have been proven very powerful in treating nuclear dynamics problems, but their naive application to electronic problems, which have a Coulomb singularity, gives poor results. This is because in the FFT method the grid has to be evenly spaced and, therefore, thousands of grid points are already needed in one-dimensional calculations [1]. Other methods like the finite element method [2–4], the expansion in complex Sturmian basis sets [6], and discrete-variable–finite-element methods [5] have been relatively successfully applied to the Coulomb problem, but lack the high efficiency of the FFT method for calculating the kinetic energy operator, which scales as $N \ln N$, where N is the number of grid points. The favorable scaling of the FFT method becomes increasingly important if N is large, as is the case when a few coupled degrees of freedom are involved.

Recently, Fattal, Baer, and Kosloff [7] used a mapped Fourier method, which combines the advantages of the finite element method and the Fourier method. It allows the placement of grid points as needed, while allowing use of the FFT for evaluation of derivatives by *mapping* the original, unevenly spaced grid to a grid that is evenly spaced. Fattal *et al.* chose the placement of the original set of grid points in such a way as to optimize the usage of the *classical* phase space, as estimated by the classical Hamiltonian with a predetermined energy cutoff. Those workers applied their method to a solution of the time-*independent* Schödinger equation using the Fourier grid Hamiltonian representation [8], and were able to calculate the first twenty bound states of the radial coordinate of the hydrogen atom very accurately, using only 64 grid points. As with earlier mappings like $x = \ln r$ [9] or $x = \sqrt{r}$ [10], Fattal *et al.* get the number of points per lobe of the wave function close to being a constant. This is because the momentum space required for the calculations fits within the range set by the Fourier method, so that the use of *phase space* is optimized rather than just the use of coordinate space. Very recently, Kokoouline *et al.* [11] applied this mapping procedure in connection with the time-independent Fourier grid Hamiltonian method to the calculation of the photoassociation spectrum of $Rb_2\,(0_u^+)$.

In the present paper, the mapped Fourier method is applied to the solution of the *time-dependent* Schrödinger equation. As a first test, the eigenstates of the hydrogen atom are extracted from spectral analysis of arbitrary wave packets evolving in a Coulomb field. Results are obtained for the one-dimensional (1D) radial Schrödinger equation, for the Schrödinger equation of the hydrogen atom in cylindrical coordinates in two degrees of freedom, and for the hydrogen atom in three degrees of freedom without using any symmetry. For extracting the eigenenergies, the filter diagonalization method developed by Wall and Neuhauser [12] and improved by Mandelshtam and Taylor [13] is applied. The second test of the time-dependent mapped Fourier method is much more severe. The ionization probability is calculated for a hydrogen atom interacting with a half-cycle pulse. First, a rectangular pulse is applied to a hydrogen atom, which is initially in an uphill or downhill Stark state with principal quantum number n; $n=5$ or $n=10$. The results are compared to the calculations of Reinhold and Burgdörfer [14] of the same quantity. Then, a more realistic pulse shape is used and the main quantum number n of the initial Stark state is increased to $n=17$. We use the same parameters as Bugacov *et al.* [15] to be able to compare directly with their results. These calculations are in close correspondence with the experiments of Jones *et al.* [16]; although the experiments are performed with sodium atoms, the theory gives good qualitative agreement for the different ionization rates of downhill and uphill states. Both calculations we compare with the one of Reinhold and Burgdörfer [14] and the one of Bugacov *et al.* [15], who use an expansion in a complex Sturmian basis. In those calculations the time-dependent Schrödinger

*Present address: Institut für Physik, Technische Universität, D-09107 Chemnitz, Germany.

 © 1999 The American Physical Society

equations are solved by a split operator technique and by an implicit Runge-Kutta algorithm, respectively. Besides the superior scaling of the mapped Fourier methods over these methods, the kinetic energy operator is also much easier to evaluate.

The paper is organized as follows. In Sec. II, the basic principles of representation theory are reviewed. In Sec. III, the general calculus of mapping and its effect on the kinetic energy operator is presented, and the particular mapping function used here is described. Section IV presents the calculation of the hydrogen atom eigenenergies, while Sec. V describes the calculation of the ionization probabilities by half-cycle pulses. Section VI gives a short summary and discussion. Atomic units are used unless otherwise stated.

II. REPRESENTATION THEORY

On a grid, a continuous wave function is represented by only a few points. Between these points an analytic set of basis functions $g_k(q)$ may be used to make a continuous description,

$$\psi(q) \approx \overline{\psi}(q) = \sum_{k=0}^{N_g-1} a_k g_k(q). \tag{1}$$

The expansion coefficients a_k are determined by matching the function $\overline{\psi}(q)$ to the true wave function $\psi(q)$ at the grid points. The relation between the grid points and expansion coefficients is called the *collocation relation* [17]. If the basis functions are orthogonal when summed over the grid points, the representation is called a *pseudospectral* representation [18]. A specific choice of basis functions, which form a pseudospectral representation, are the complex exponentials

$$g_k(q) = e^{i2\pi kq/L}, \quad k = -N_g/2, \ldots, 0, \ldots, N_g/2-1 \tag{2}$$

This method is named the Fourier method. Since the method is pseudo spectral one gets

$$a_k = \frac{1}{N_g} \sum_{j=1}^{N_g} \psi(q_j) e^{-i2\pi kp_j/L}. \tag{3}$$

An appealing feature of this representation is the physical meaning of the coefficients a_k as the discrete representation of the wave function in momentum space. The grid points in the Fourier method are equally spaced, with spacing $\Delta q = L/N_g$ in coordinate space and with spacing $\Delta k = 2\pi/L$ in momentum space.

The accuracy of the Fourier representation is determined by the Whittaker-Kotel'nikov-Shannon sampling theorem [19,20]. The theorem states that band limited functions (i.e., functions that are compact in momentum space), that have finite support (i.e., which are compact in coordinate space) can be interpolated with no loss of accuracy provided that $\Delta q < \pi/k_{max}$. The function values in between the grid points are interpolated by

$$\psi(q) = \sum_{-(N_g/2-1)}^{N_g/2} \psi(n\Delta q) \frac{\sin[k_{max}(q-n\Delta q)]}{k_{max}(q-n\Delta q)}. \tag{4}$$

This theorem also implies a good representation of the nth derivative of the function. It can be shown that the best band limited functions are prolate spheroidal wave functions [20]. These functions are not easy to handle, and a much simpler but still good set of wave functions are Gaussian wave functions. Their amplitude outside a finite size interval can be made exponentially small in both coordinate and momentum space. One can define a wave packet as a wave function, which is semilocal in phase space.

Wave functions in general are not strictly band limited and have no finite support in coordinate space. In the general case, one may analyze the efficiency of the representation with the help of the classical or the Wigner-Weyl phase space [21]. The phase space in the Fourier method has a rectangular shape and its volume is [17]

$$\mathcal{V} = 2\hbar L k_{max} = N_g h. \tag{5}$$

So at most N_g quantum states can be represented on the grid. If only N_e converged eigenstates are represented, the representation efficiency is

$$\eta_c = \frac{N_e}{N_g}. \tag{6}$$

Because quantum wave functions decay exponentially outside the classically accessible phase-space Ω, a good estimate of the representation efficiency is given by the ratio of the classical phase-space volume, which is accessible to the phase-space volume of the Fourier grid

$$\eta_c \approx \frac{\Omega}{N_g h}. \tag{7}$$

The main idea of the mapping procedure proposed by Fattal, Baer, and Kosloff [7] is the use of Eq. (7). The mapping parameters are chosen in such a way that the efficiency given by Eq. (7) is maximal. This gives a physically motivated mapping, which can be determined before the actual calculation.

III. MAPPING PROCEDURE

The mapping should be a canonical mapping from the N canonical Cartesian coordinates $\{q_i\}$ to the N curvilinear coordinates $\{Q_i\}$. The original coordinates are always given in small letters throughout the paper, whereas the mapped coordinates, on the evenly spaced grid, are given in capital letters. Typically, a mapping function is defined, which depends on a small number of discrete parameters. The Riemann metric tensor is given by

$$g_{ij} = \sum_k \frac{\partial q^k}{\partial Q^i} \frac{\partial q^k}{\partial Q^j}, \tag{8}$$

the Jacobian is given by

$$J = \sqrt{\det(g_{ij})}, \tag{9}$$

and the transformed Laplacian is given by [22]

$$\Delta = \frac{1}{J} \sum_j \frac{\partial}{\partial Q^j} \sum_k \left(J g^{jk} \frac{\partial}{\partial Q^k} \right). \tag{10}$$

The use of such a mapping in electronic structure calculations was pioneered by Gygi [23]. For atomic systems with empirical mapping parameters a mapping of coordinates was also recently done by Andrae and Hinze [24]. A mapping function similar to that of Gygi has been used by Fattal, Baer, and Kosloff [7] for the radial coordinate of the hydrogen atom

$$q = N[Q - A \arctan(\beta Q)], \tag{11}$$

with N being a constant that keeps the length of the grid fixed. For small values of Q this function behaves like

$$q = N(Q - A\beta Q + \tfrac{1}{3} A\beta^3 Q^3 + \cdots). \tag{12}$$

Choosing $A\beta \approx 1$ makes the coordinate q behave like a cubic function of Q for small values of Q. Therefore, with an equally spaced grid in Q, there will be a lot of points near the singularity $q=0$ (see Fig. 2 of Ref. [7]). For numerical reasons, the product $A\beta$ has to be a little less than unity and its actual deviation from unity is related to the strength of the mapping function.

Earlier calculations [23,25,26] used adaptive methods to calculate the mapping parameters. In contrast to this, Fattal *et al.* maximized the representation efficiency of the grid, i.e., maximized η_c in Eq. (7), before the actual calculation. For a fixed number of grid points, N_g, this is done by maximizing $\Omega = \int p\,dq$. For the mapping function, Eq. (11), and fixed product, $A\beta$, the integral is a smooth function of the parameter β and reaches a plateau, which can be obtained easily. The results are quite insensitive to the exact value of β. However, because the ratio of the energy cutoff of the grid with mapping and without mapping goes like

$$\frac{E_{mapped}}{E_{unmapped}} \propto \left(\frac{N_g}{\beta L} \right)^4, \tag{13}$$

it is preferable to choose the smallest possible value of β after the plateau is reached. For figures of the classical energy shell and the Wigner function with and without mapping, see Ref. [7].

The mapping function, Eq. (11), can be extended to higher dimensions in different ways. The simplest possibility is to do the mapping in every coordinate separately,

$$q_i = N[Q_i - A \arctan(\beta Q_i)] \tag{14}$$

or to perform a global mapping that depends on the distance ρ from the nucleus

$$q_i = N Q_i [1 - f(\rho)],$$

$$f(\rho) = \frac{A}{\rho} \arctan(\beta\rho), \tag{15}$$

$$\rho = \sqrt{Q_1^2 + Q_2^2 + \cdots}.$$

The first choice is much easier to implement because the metrical tensor g_{ij} is diagonal and the mapping parameter can be determined separately for each dimension. How to determine the optimal mapping parameter for the second possibility, Eq. (15), is not obvious (work in this direction is in progress). For atomic problems, the efficiencies of the two different mapping procedures were found not to differ much. This was tested by small time-independent calculations where the mapping parameter could be determined variationally. For cylindrical coordinates the first procedure is superior because the wave functions change a lot along the z axis. Therefore, a fine grid along this line, as created by the first mapping procedure, Eq. (14), is always advantageous. In three dimensions both procedures performed equally well for small systems, even when the mapping parameters were determined variationally.

IV. EXTRACTING THE EIGENENERGIES OF A HYDROGEN ATOM

A. Radial Schrödinger Equation

First we use the full spherical symmetry of the hydrogen atom, i.e., we write the solution as

$$\Psi_{nlm}(r,\theta,\phi) = \Phi(r) Y_{lm}(\theta,\phi) \tag{16}$$

with $Y_{lm}(\theta,\phi)$, the spherical harmonics. After the substitution $\phi(r) = \Phi(r)/r$, the radial Hamiltonian is given by

$$H = -\frac{1}{2}\frac{\partial^2}{\partial q^2} - \frac{1}{q} + \frac{l(l+1)}{2q^2}. \tag{17}$$

In the mapped coordinate Q the Hamiltonian is given by

$$H = -\frac{1}{2}\left(J^{-1}\frac{\partial}{\partial Q} \right)^2 - \frac{1}{N[Q - A\arctan(\beta Q)]} + \frac{l(l+1)}{2\{N[Q - A\arctan(\beta Q)]\}^2}. \tag{18}$$

For evaluating this kinetic energy operator within the Fourier method, four FFTs are needed since $J^{-1}(Q)$ is local in coordinate space. By using the identity

$$\left(J^{-1}\frac{\partial}{\partial Q} \right)^2 = J^{-1}\left(J^{-1}\frac{\partial}{\partial Q} + \frac{\partial J^{-1}}{\partial Q} \right)\frac{\partial}{\partial Q}, \tag{19}$$

the number of FFTs needed can be reduced to three, since the derivative of J^{-1} can be evaluated analytically. The use of three instead of four FFTs does not affect the accuracy significantly for one evaluation of the Hamiltonian H on a wave function; however, if many evaluations are needed, e.g., to build up a Krylov space ($\Psi_n = H^n \Phi_0$) for time propagation, the version with four FFTs was found to be much more stable. Using the transformation described in Ref. [24] it is possible to use only two FFTs; however, this transformation generates an additional potential energy term with much more structure than the Coulomb potential, so that for the same number of grid points one actually gets less accurate results this way. Therefore in all calculations described in this paper four FFTs were used for evaluating the kinetic energy operator.

TABLE I. Eigenenergies of atomic hydrogen in atomic units (for convenience the minus sign has been neglected). The second column gives the exact values, whereas the other three columns give values from time-dependent runs. For the calculations in the third column, spherical symmetry has been used; for the fourth column, cylindrical symmetry; and for the last column, no symmetry at all. The 1D and 2D runs have been optimized for eigenstates with n up to 20, the 3D run for n up to 10.

	Exact	Mapping		
Dimension		1D	2D	3D
N_g		64	64^2	32^3
L		1600	1600	400
1	0.500 0000	0.499 91	0.499 92	
2	0.125 00	0.125 01	0.125 01	
3	5.556×10^{-2}	5.5557×10^{-2}	5.5557×10^{-2}	5.5520×10^{-2}
4	3.1250×10^{-2}	3.1245×10^{-2}	3.1245×10^{-2}	3.1265×10^{-2}
5	2.0000×10^{-2}	2.0003×10^{-2}	2.0003×10^{-2}	2.0030×10^{-2}
6	1.3889×10^{-2}	1.3887×10^{-2}	1.3887×10^{-2}	1.3884×10^{-2}
7	1.0204×10^{-2}	1.0203×10^{-2}	1.0203×10^{-2}	1.0217×10^{-2}
8	7.8125×10^{-3}	7.8118×10^{-3}	7.8118×10^{-3}	7.8924×10^{-3}
9	6.1723×10^{-3}	6.1724×10^{-3}	6.1724×10^{-3}	
10	5.0000×10^{-3}	4.9997×10^{-3}	4.9997×10^{-3}	
11	4.1322×10^{-3}	4.1320×10^{-3}	4.1320×10^{-2}	
12	3.4722×10^{-3}	3.4721×10^{-3}	3.4721×10^{-3}	
13	2.9586×10^{-3}	2.9585×10^{-3}	2.9585×10^{-3}	
14	2.5510×10^{-3}	2.5507×10^{-3}	2.5507×10^{-3}	
15	2.2222×10^{-3}	2.2222×10^{-3}		
16	1.9531×10^{-3}	1.9529×10^{-3}		
17	1.7301×10^{-3}	1.7306×10^{-3}		

The time propagation was performed using the short iterative Lanczos (SIL) propagator [27]. This propagator allows for mixed terms of P and Q in the kinetic energy operator, as introduced by the mapping. The split operator technique [28] often used for time propagation does not allow for mixed terms of P and Q and, therefore, cannot be used here. An additional advantage of the SIL comes from consideration of the energy spectrum of the mapped grid. The curvature of the mapping function introduces high energy components to the grid energies. Typically, these high energy components have very little amplitude, but can still lead to numerical instability [29] unless a time step on the order of $\Delta t = N/\Delta E$ is used, with N being the order of the propagator and ΔE, the spectral range of the Hamiltonian. This instability is characteristic of the Chebyshev propagation method and other uniform methods. The Lanczos method is unconditionally stable; moreover, the error is determined only by the component of the initial state at these high energy regions of the spectrum, which is typically on the order of 10^{-12}. Unfortunately, for very long propagation times as used in Sec. V, these small components at high energies reduce the typical time step to a value of 2–3 times longer than the time step of a Chebychev propagator [30]. Attempts to get rid of those components at high energies in Krylov space failed because they reoccur after a few Lanczos iterations or because these methods are too time consuming [30].

For the extraction of the eigenenergies, the autocorrelation function $S(t) = \langle \phi(0) | \phi(t) \rangle$ has to be calculated. Since the Hamiltonian is time-independent a trick can be used to construct $S(2t)$ out of the wave function at time t [31],

$$S(2t) = \langle \phi(0) | \phi(2t) \rangle = \langle \phi^*(t) | \phi(t) \rangle. \tag{20}$$

The most common way to extract energies out of the autocorrelation function is by standard Fourier transform [32], but this requires propagation of the wave packet for a time $t \geqslant 1/\Delta E$, where ΔE is the energy separation between the desired state and its nearest neighbor. A method far superior to this is the filter diagonalization method first developed by Wall and Neuhauser [12] and improved by Mandelshtam and Taylor [13]; the latter version is used here. The basic idea is to fit a time signal to a sum of complex exponentials, where the fitting parameters are the complex amplitudes and frequencies. In general, this is a difficult nonlinear search in a many-dimensional space; the significance of Wall and Neuhauser's work was to show how this problem could be turned into a small linear algebra problem.

Table I shows the eigenenergies of the radial Schrödinger equation in comparison with the exact eigenenergies. Atomic units are used, in which $E_n = -1/(2n^2)$. The grid was optimized to represent the first 20 eigenstates. As can be seen in Table I, the accuracy is quite good. The remaining error is not due to the time propagation but due to the representation error incurred by the use of a finite grid. The energies were obtained by propagating arbitrary Gaussian wave packets on the grid, and extracting their spectral frequencies via filter diagonalization. Typically, the wave packets were propagated for a time of 10 000 a.u., after which the filter diagonalization method gives converged energies. A time step of 1 a.u. was used. Generally, the propagation of one wave packet is not enough because it does not have enough overlap with all the desired eigenstates. Therefore, a few different starting wave packets need to be propagated. These results already show that the mapped Fourier method is not limited to time-

independent calculations but can also be used efficiently within a time-dependent framework. The real advantages, however, will become apparent in higher dimensional problems below.

A. Cylindrical coordinates

This subsection shows how the mapping in cylindrical coordinates can be combined with time propagation. This is especially important for atoms in linearly polarized fields and diatomic molecules. The time-independent version of the mapping was already used successfully to calculate the eigenenergies of the hydrogen molecular ion in [7]. The calculation of ionization rates in a linearly polarized electric field is described in the next section. The transformation from Cartesian to cylindrical coordinates and the mapping are combined into a single step here. The original Cartesian coordinates ($\{q_i\}$) will be called x, y, and z here and the mapped cylindrical coordinates ($\{Q_i\}$) R, Z, and Φ:

$$x = N_R[R - A_R \arctan(\beta_R R)]\cos\Phi, \tag{21a}$$

$$y = N_R[R - A_R \arctan(\beta_R R)]\sin\Phi, \tag{21b}$$

$$z = N_Z[Z - A_Z \arctan(\beta_Z Z)]. \tag{21c}$$

The coordinates R and Z are mapped in the same way as the coordinate q in the radial Schrödinger equation. The azimuthal coordinate Φ is not mapped and is of no concern because we are interested in problems with azimuthal symmetry here. Using the abbreviations

$$J_1 = N_R\left(1 - \frac{\beta_R A_R}{1 + (\beta_R R)^2}\right), \tag{22a}$$

$$J_2 = N_R[R - A_R \arctan(\beta_R R)], \tag{22b}$$

$$J_3 = N_Z\left(1 - \frac{\beta_Z A_Z}{1 + (\beta_Z Z)^2}\right), \tag{22c}$$

the metric tensor looks like

$$g = \begin{pmatrix} J_1^2 & 0 & 0 \\ 0 & J_2^2 & 0 \\ 0 & 0 & J_3^2 \end{pmatrix} \tag{23}$$

and the Jacobian

$$J = \sqrt{|g|} = J_1 J_2 J_3. \tag{24}$$

Because of the azimuthal symmetry the wave function can be written as

$$\Psi(R,Z,\Psi) = \phi(R,Z)e^{im\Phi} \tag{25}$$

and so the Laplacian is given by

$$\Delta = \frac{1}{J_1 J_2}\frac{\partial}{\partial R}\left(\frac{J_2}{J_1}\frac{\partial}{\partial R}\right) + \frac{1}{J_3}\frac{\partial}{\partial Z}\left(\frac{1}{J_3}\frac{\partial}{\partial Z}\right) - \frac{m^2}{J_2^2}. \tag{26}$$

Since the mappings in R and Z are completely decoupled, the mapping parameters A_R, β_R and A_Z, β_Z can be determined separately. Each of these parameters can be calculated in the same way as described for the radial Schrödinger equation. Again, the grid is constructed to represent the first 20 eigenstates accurately. A time step of 0.5 a.u. is used with a total propagation time of 10 000 a.u. The eigenenergies are extracted and listed in Table I. Once more the error is due to the limits of the grid representation and not due to time propagation. This calculation indicates that the mapping is efficient also for propagation in cylindrical coordinates.

B. Full 3D calculation

Finally, we show that with the mapping it is possible to do a time-dependent Fourier propagation in the Coulomb potential without using any symmetry. For simplicity, we perform the mapping in each Cartesian coordinate separately as given by Eq. (14). Again, the mapping parameters can be determined as in the case of the radial Schrödinger equation. The metrical tensor g is diagonal and the Jacobian is just a product of three Jacobians of the form used in the radial Schödinger equation. The results are quite accurate, as seen in Table I. It is worth noting that the 1-D radial Schrödinger equation could have been solved using the Fourier method without mapping, but this would have required thousands of grid points. However, without mapping, the 2-D calculations are already beyond the capabilities of current computers and the 3-D calculations are beyond the capabilities of any computers projected for the next generation. In 3-D, the time-dependent calculations of the eigenenergies start to have significant advantages over the time-independent methods. This is because in time-independent methods huge Hamiltonian matrices have to be set up and to be diagonalized. This is not the case in time-dependent calculations, which operate only with vectors of the form $H\Psi$.

V. IONIZATION BY HALF-CYCLE PULSE

Until now no external field was involved in the calculations. As a next test we apply the time-dependent version of the mapped Fourier method to the hydrogen atom in the presence of a half-cycle pulse. Half-cycle pulses are especially interesting because they can ionize a Rydberg wave packet far away from the core. A variety of experiments on alkali-metal atoms with half-cycle pulses have been performed recently [33,16]. In some experiments [16] a very weak static electric field F_{dc} was aligned along the positive z axis. This field splits the Rydberg manifold into Stark states [34]. For pure hydrogenic systems the Stark states are eigenstates of the Hamiltonian in parabolic coordinates with the quantum numbers n_1, n_2, and m. The principal quantum number n is given by $n = n_1 + n_2 + |m| + 1$. The energies of the Stark states within the static field are $(3/2Z)n(n_1 - n_2)F_{dc}$. For $n_1 > n_2$ the electron is mainly on the positive side of the z axis and therefore on the uphill side of the small potential F_{dc}. These states are called uphill states. For $n_1 < n_2$ the electron is mainly on the negative side of the z axis; these are called the downhill states. As in the experiment, only the most uphill ($n_1 = n-1$, $n_2 = 0$) and the most downhill ($n_1 = 0$, $n_2 = n-1$) states are considered. The very weak field F_{dc} can be neglected in the calculations.

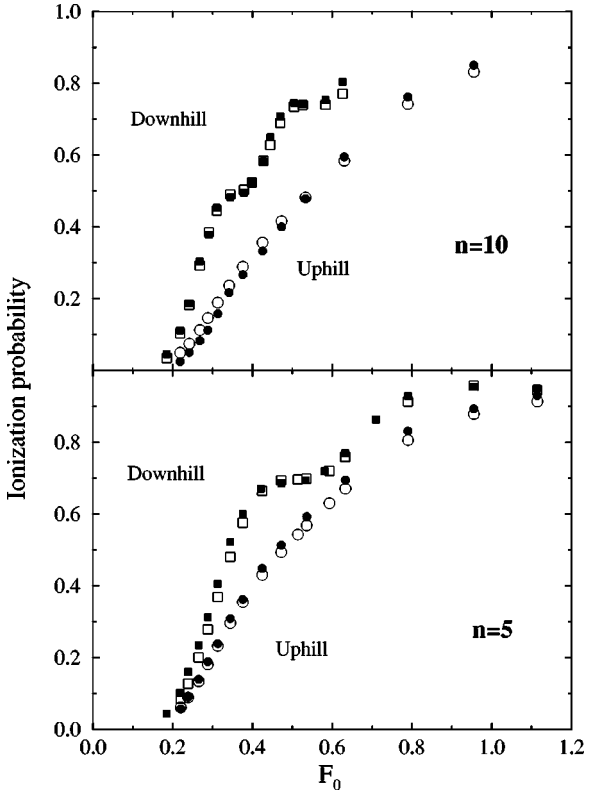

FIG. 1. Ionization probability for the extreme Stark states with $n=5$ as well as $n=10$ and $m=0$. The filled symbols show the results by Reinhold and Burgdörfer [14] and the open symbols show the present calculations. Circles refer to the most uphill states and squares refer to the most downhill states.

The half-cycle pulse is first modeled by a rectangular pulse $[F(t)=F_p$ for $0<t<T_p]$ with a scaled peak field $F_0=n^4F_p$ and a scaled pulse duration $T_0=T_p/T_n=T_p/(\pi n^3)=0.5$. The parameters are chosen as in the article by Reinhold and Burgdörfer [14]. The ionization rate is calculated as one minus the bound state rate

$$P_{ion}=1-\sum_{n=1}^{N}\sum_{l=0}^{n-1}|\langle\phi_{nl,m=0}|\psi(T_p)\rangle|^2. \tag{27}$$

Figure 1 shows the present results in comparison to the results of Reinhold and Burgdörfer [14]. The agreement is very good. The small deviations most probably result from different ways of determining the ionization rate. In the present calculation the final wave packet was projected onto bound states with main quantum numbers up to $n=35$.

Due to experimental difficulties it is hard to create a pure half-cycle pulse. In addition to the strong positive lobe the experimental pulses also have a long but much weaker negative tail. We repeat the calculations of Bugacov *et al.* [15], which incorporate this more realistic form for the pulse shape. Those workers used a different technique, expanding the wave function into a Sturmian basis and integrating by a Runge-Kutta algorithm. The pulse profile is given by [15]

$$F(t)=0, \quad t<0 \tag{28a}$$

$$F(t)=29.56F_0[17.75(t/\tau)^3e^{-8.87/\tau}-0.412(t/\tau)^5e^{-4.73/\tau}], \quad t\geq 0 \tag{28b}$$

with $\tau=1$ psec, approximating the form of the experimental pulse. The initial state is taken as $n=17$. After the pulse is over the wave packet is projected onto the bound states. At the edges of the grid the wave functions are multiplied by a damping function to avoid reflection or wrap around. The damping function used has the form [35]

$$f(x_i)=\sin^2\left(\frac{\pi}{2}\frac{(x_{mask}+\Delta x_{mask}-x_i)}{\Delta x_{mask}}\right), \quad x_i\geq x_{mask} \tag{29}$$

x_{mask} is the point at which the masking function is initiated and $\Delta x_{mask}=x_{max}-x_{mask}$ is the width over which the function decays from 1 to 0 with x_{max} being the maximum length of the grid in that direction.

The determination of the mapping parameter β is not as clear as it was in the case of the bound state calculations without electric field. A good starting point is to use the same procedure as described in Sec. III, but then the grid must be extended in coordinate as well as in momentum space to allow for the evolution of the wave packet due to the pulse. To reduce the grid range needed in momentum space the velocity gauge was used, i.e., the Hamiltonian in unscaled coordinates reads

$$H=\frac{1}{2}(\vec{p}-\vec{A})^2-\frac{1}{r} \tag{30}$$

with the vector potential $\vec{A}$ given by

$$\vec{A}(t)=-\int^t\vec{E}(t')dt'. \tag{31}$$

This gauge is advantageous compared with the length gauge because it compensates for much of the momentum transferred from the pulse to the electron. Still, there was some intensity in the momentum distribution near $R=0$. To deal a little better with this effect, an additional constant shift in momentum space was introduced.

Figure 2 shows the comparison of the present results with those of Bugacov *et al.* [15]. Again, the ionization rate was calculated by projecting onto bound states but this time many more bound states were required. For the downhill states, projecting onto about 80 bound states gave converged results but for the uphill states about 150 bound states were required. This is because the wave function in the uphill state scatters from the core before ionization, and therefore is pushed into high-n states. In Fig. 2, only those points of Bugacov *et al.* which were calculated explicitly, are shown [36]. In Ref. [15], these points were connected with smooth lines that is fine for the uphill initial state, but misleading for the downhill initial state, where the full curve oscillates as a function of energy. The oscillations can be traced to the effective one-dimensional ionization of the downhill states, which contrasts with the bona fide two-dimensional ionization of the uphill states, as discussed in [14]. The converged calculations required 432 points in the z direction and 96

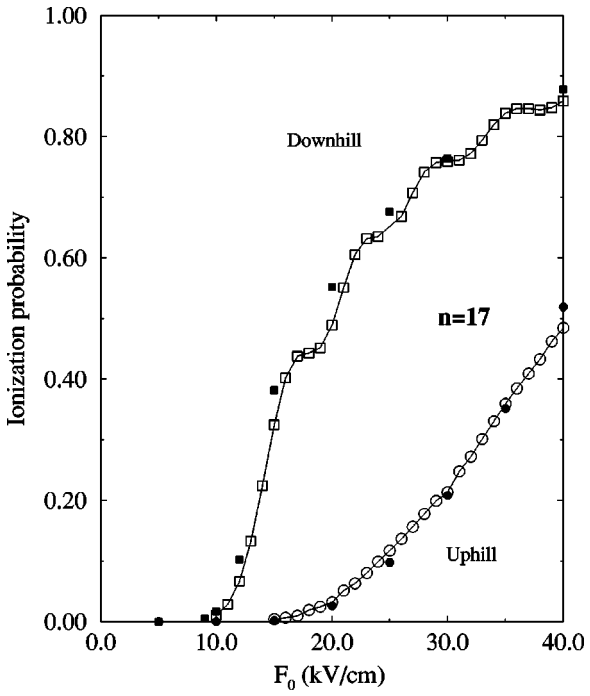

FIG. 2. Ionization probability for the extreme Stark states with $n=17$ and $m=0$. The filled symbols show the results by Bugacov *et al.* [15] and the open symbols show the present calculations.

points in the r direction. Absorbing boundary conditions were used to reduce the grid range.

The calculation of the ionization rate in Fig. 2 required projecting onto hundreds of bound states, represented numerically on the grid. This projection procedure could potentially have introduced significant numerical errors into the calculation. A similar numerically intensive projection procedure was required by Bugacov *et al.* [15]. Under the circumstances, the degree of agreement with the results of Bugacov *et al.* is very gratifying, to the point of being almost surprising.

VI. CONCLUSIONS

We have shown in this paper that the mapped Fourier method as developed by Fattal *et al.* [7] can be extended to time-dependent calculations. As in the time-independent method, the mapping leads to a much more efficient representation of the phase space on an evenly spaced grid of points. As we have applied it here, the mapped Fourier method is optimized only for a certain number of bound states. However, for a general time-dependent Hamiltonian, the spectral components of the wave packet change in time, and it is difficult to estimate the phase space that will be needed in advance. Moreover, in the presence of ionization or dissociation the phase space is unbound. Nevertheless, we have shown in this paper that the method can still be applied profitably to these types of problems.

ACKNOWLEDGMENTS

We thank Ronnie Kosloff and Eyal Fattal for many helpful suggestions. We are grateful to V. S. Mandelshtam for providing us with his filter diagonalization code. U.K. wishes to thank the Minerva Stiftung, under which this work was done, for financial support.

[1] R. Dehnen and V. Engel, Phys. Rev. A **52**, 2288 (1995).
[2] H. Yu and A.D. Bandrauk, J. Chem. Phys. **102**, 1257 (1995).
[3] E. Huens, B. Piraux, A. Bugacov, and M. Gajda, Phys. Rev. A **55**, 2132 (1997).
[4] S. Yoshida, C.O. Reinhold, J. Burgdörfer, B.E. Tannian, R.A. Popple, and F.B. Dunning, Phys. Rev. A **58**, 2229 (1998).
[5] W. Schweizer and P. Faßbinder, Comput. Phys. **11**, 641 (1997).
[6] M. Pont, D. Proulx, and R. Shakeshaft, Phys. Rev. A **44**, 4486 (1991).
[7] E. Fattal, R. Baer, and R. Kosloff, Phys. Rev. E **53**, 1217 (1996); E. Fattal, Ph.D. thesis, Hebrew University, Jerusalem, 1996.
[8] C.C. Marston and G.B. Balint-Kurti, J. Chem. Phys. **91**, 3571 (1989).
[9] M.L. Zimmerman, M.G. Littman, M.M. Kash, and D. Kleppner, Phys. Rev. A **20**, 2251 (1979).
[10] S.A. Bhatti, C.L. Cromer, and W.E. Cooke, Phys. Rev. A **24**, 161 (1981).
[11] V. Kokoouline, O. Dulieu, R. Kosloff, and F. Masnou-Seeuws, J. Chem. Phys. **110**, 9865 (1999).
[12] M.R. Wall and D. Neuhauser, J. Chem. Phys. **102**, 8011 (1995).
[13] V.A. Mandelshtam and H.S. Taylor, Phys. Rev. Lett. **78**, 3274 (1997).
[14] C.O. Reinhold and J. Burgdörfer, Phys. Rev. A **51**, R3410 (1995).
[15] A. Bugacov, B. Piraux, M. Pont, and R. Shakeshaft, Phys. Rev. A **51**, 4877 (1995).
[16] R.R. Jones, N.E. Tielking, D. You, C. Raman, and P.H. Bucksbaum, Phys. Rev. A **51**, R2687 (1995).
[17] R. Kosloff, in *Numerical Grid Methods and Their Application to Schrödinger's Equation*, edited by C. Cerjan (Kluwer, Dordrecht, 1993).
[18] D. Gottlieb and S. A. Orszag, *Numerical Analysis of Spectral Methods: Theory and Applications* (SIAM, Philadelphia, 1977).
[19] E.T. Whittaker, Proc. R. Soc. Edinburgh **35**, 181 (1915); H. Nyquist, Trans. Am. Inst. Electr. Eng. **47**, 617 (1928); C. E. Shannon, Proc. IRE **37**, 10 (1949).
[20] A. Papoulis, *The Fourier Integral and its Applications* (McGraw-Hill, New York, 1962).
[21] E.P. Wigner, Phys. Rev. **40**, 749 (1932); M. Hillery, R.F. O'Connel, M.O. Scully, and E.P. Wigner, Phys. Rep. **106**, 121 (1984).
[22] A. Visconti, *Introductory Differential Geometry for Physicists* (World Scientific, Singapore, 1992).
[23] F. Gygi, Europhys. Lett. **19**, 617 (1992); Phys. Rev. B **48**, 11 692 (1993).
[24] D. Andrae and J. Hinze, Int. J. Quantum Chem. **63**, 65 (1997).
[25] F. Gygi, Phys. Rev. B **51**, 11 190 (1995); F. Gygi and G. Galli, *ibid.* **52**, R2229 (1995).
[26] G. Zumbach, N.A. Modine, and E. Kaxiras, Solid State Com-

mun. **99**, 57 (1996); N. A. Modine, G. Zumbach, and E. Kaxiras, in *Materials Theory, Simulations, and Parallel Algorithm*, edited by E. Kaxiras, J. Joannopoulos, P. Vashishta, and R. Kalia, MRS Symposia Proceedings No. 408 (Materials Research Society, Pittsburgh, 1996), p. 139; N.A. Modine, G. Zumbach, and E. Kaxiras, Phys. Rev. B **55**, 10 289 (1997).

[27] C. Leforestier, R.H. Bisseling, C. Cerjan, M.D. Feit, R. Friesener, A. Guldberg, A. Hammerich, G. Jolicard, W. Karrlein, H.-D. Meyer, N. Lipkin, O. Roncero, and R. Kosloff, J. Comput. Phys. **94**, 59 (1991).

[28] M.D. Feit, J.A. Fleck,Jr., and A. Steiger, J. Comput. Phys. **47**, 412 (1982); M.D. Feit and J.A. Fleck, Jr., Appl. Opt. **17**, 3990 (1978); **18**, 2843 (1979); **19**, 1154 (1980); **19**, 2240 (1980).

[29] J. K. Cullum and R. A. Willoughby, *Lanczos Algorithms for Large Symmetric Eigenvalue Computations* (Birkhäuser, Boston, 1985), Vol. I.

[30] R.E. Wyatt, Phys. Rev. E **51**, 3643 (1995); G. Jolicard, A. Grosjean, and J.P. Killingbeck, J. Chem. Phys. **105**, 5939 (1996); P.-N. Roy and T. Carrington, Jr., *ibid.* **103**, 5600 (1995).

[31] V. Engel, Chem. Phys. Lett. **189**, 76 (1992).

[32] M.D. Feit, J.A. Fleck, Jr., and A.J. Steiger, J. Comput. Phys. **47**, 412 (1982).

[33] R.R. Jones, D. You, and P.H. Bucksbaum, Phys. Rev. Lett. **70**, 1236 (1993); R.R. Jones, *ibid.* **76**, 3927 (1996).

[34] H. A. Bethe and E. E. Salpeter, *Quantum Mechanics of One- and Two-Electron Atoms* (Springer-Verlag, New York, 1957).

[35] S. Mahapatra and N. Sathyamurthy, J. Chem. Soc., Faraday Trans. **93**, 773 (1997).

[36] R. Shakeshaft (private communication).